Progress In Electromagnetics Research M, Vol. 89, 63–71, 2020

A Filtering Dielectric Resonator Antenna with High Band-Edge Selectivity

Yang Gao, Yong-Chang Jiao, Zibin Weng*, Chi Zhang, and Yi-Xuan Zhang

Abstract—A filtering rectangle dielectric resonator antenna (DRA) with high band-edge selectivity is proposed in this paper. The DRA is fed by a simple hybrid feeding structure consisting of a microstrip-coupled slot on the bottom and a thin metallic strip on the side of DRA to excite the fundamental $\mathrm{TE}^{y}_{1\delta 1}$ mode. The feeding structure establishes a cross-coupled mechanism which includes electric and magnetic coupling. This mechanism introduces two radiation nulls at the band edge without any filtering circuits. By using the designed hybrid feeding structure, a bandpass filtering response is obtained. For enhancing band-edge selectivity, a shorted stub is introduced to weaken the coupling between the two microstrip stubs of the feeding structure. A wide impedance bandwidth of 19% and a flat gain around 5.6 dBi are realized. To validate the proposed design, a prototype is fabricated and measured, showing a favorable agreement with the simulated results.

1. INTRODUCTION

Filters and antennas are fundamental components that are extensively used in wireless communication systems [1]. As modern technologies are developing rapidly, miniaturization and integration are significantly demanded for RF front-end receivers. Therefore, antennas integrated with filters called filtering antennas are widely needed [2].

In recent years, there are mainly three methods for designing filtering antennas. One of the methods is co-design scheme [3, 4]. In this way, filtering circuits and antennas are directly connected by using extra impedance transformers, which inevitably increases the size and introduces extra losses. Additionally, some designs are realized by using antenna radiators to replace the last-stage resonators of filters, and the method is called filter synthesis approach [5, 6]. However, these multiple resonators are big in size. This method also needs to extract the external quality factor of the filters, which is complex in design. The third method is called antenna fusion approach. Some special parasitic or resonant structures are introduced into antennas, generating some radiation nulls and bandpass responses in the reflection coefficient and gain curves of these antennas [7, 8]. One of the advantages of this method is that it does not increase the sizes of antennas.

Dielectric materials can be used as radiators of antenna, which are called dielectric resonator (DR) antennas (DRAs) [9]. DRAs have attracted much attention owing to their advantages such as low loss, high efficiency and easy excitation [10, 11]. Recently, many filtering dielectric resonator antennas have been proposed [12–16]. The first filtering DRA design was proposed in [12]. It introduced a pair of separated slots, a pair of parasitic strips parallel to the microstrip line and an extended microstrip line to generate two radiation nulls. The filtering function was implemented by introducing a filtering balun and a four-leaf-clover which was shaped to generate out-of-phase E-filed inside the DRA [13]. In [14, 15], hybrid feeding structures were introduced to establish cross coupling to generate radiation nulls. Moreover, a compact quasi-isotropic DRA with a filtering response was proposed in [16]. Two

Received 27 November 2019, Accepted 11 January 2020, Scheduled 27 January 2020
* Corresponding author: Zibin Weng (zibinweng@mail.xidian.edu.cn).
The authors are with the National Key Laboratory of Antennas and Microwave Technology, Xidian University, Xi'an 710071, China.

radiation nulls were generated by utilizing a slot and two stubs with different sizes. However, the band-edge selectivity of the above designs were poor which influences the filtering characteristics.

Based on previous research, a filtering rectangle dielectric resonator antenna with high band-edge selectivity is proposed in this paper. It is fed by a simple hybrid feeding structure consisting of a microstrip-coupled slot and a thin metallic strip. The metallic strip can establish the electric coupling while the microstrip-coupled slot establishes the magnetic coupling. The feeding mechanism excites the fundamental $TE^{y}_{1\delta1}$ mode of a rectangle dielectric resonator. The connecting structure between the thin metallic strip and the two open stubs is utilized to establish cross coupling to generate two radiation nulls at the edges of its passband. Another shorted stub is introduced to improve the band-edge selectivity. As a result, a DRA with a bandpass filtering response is realized without any filtering circuits. Also, the reflection coefficient and broadside gain at the band edges show a good roll-off rate, while a flat gain around 5.6 dBi in the passband is obtained for the proposed DRA.

2. ANTENNA CONFIGURATION AND MECHANISM

2.1. Antenna Configuration

The configuration of proposed DRA is shown in Figure 1. Its radiating structure is a rectangular dielectric resonator with side length L, height h, and high relative permittivity $\varepsilon_{r1} = 9.5$. The substrate of the antenna is with side length G, height h_s, and relative permittivity $\varepsilon_{r2} = 3.38$. The DRA is fed by a hybrid feeding structure consisting of a thin metallic strip and a microstrip-coupled slot. In Figure 1(a), the thin metallic strip with length l_f and width w_f is on the sidewall of DRA, which establishes the electric coupling. As shown in Figure 1(b), three stubs with lengths l_{s1}, l_{s2}, l_{s3} and widths w_{s1}, w_{s2}, w_{s3} are located at the bottom layer of the substrate and connected to a stair-shaped microstrip feedline. The middle stub is shorted to the ground at its end through a shorted via. The stair-shaped microstrip feedline is used for better impedance matching. The gaps between the three stubs are g_1 and g_2. Besides, a metallic ground plane with the same size of the substrate has a slot with width w_s and length l_s, which is located at the top layer of the substrate. The coupling slot and the two open stubs establish the magnetic coupling. Both the dielectric resonator and the coupling slot are in the middle of the metallic ground plane. By keeping the slot dimensions electrically small, the amount of radiation spilling beneath the ground plane can be minimized [17]. Besides, a via in the substrate is used to connect the microstrip feedline and the thin metallic strip. The parameters of the proposed DRA are shown in Table 1.

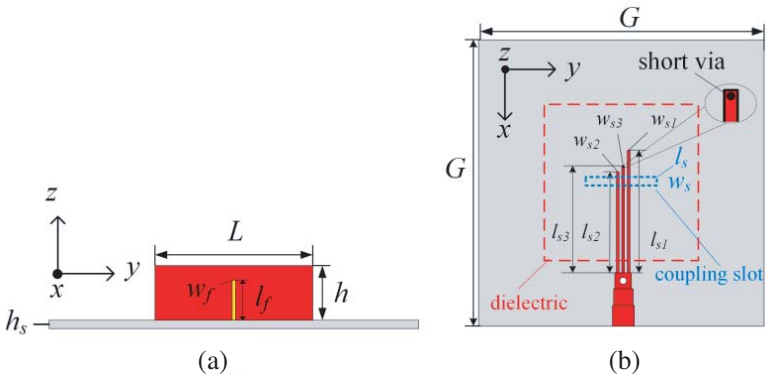

Figure 1. Configuration of the rectangular dielectric resonator antenna. (a) Thin metallic strip (electric coupling path) and (b) microstrip-coupled slot (magnetic coupling path).

2.2. Simulated Results

The simulated results of antenna performance are conducted by HFSS. Figure 2 shows a comparison of the reflection coefficient and realized broadside gain between a conventional feeding DRA and the

Table 1. Parameters of the proposed antenna (units: mm).

L	G	h	h_s	w_f	l_f
45	72	17.5	0.8	0.1	17
w_{s1}	l_{s1}	w_{s2}	l_{s2}	w_{s3}	l_{s3}
0.2	29.6	0.4	22.1	0.4	0.4
l_s	w_s	g_1	g_2		
3	1	0.1	0.26		

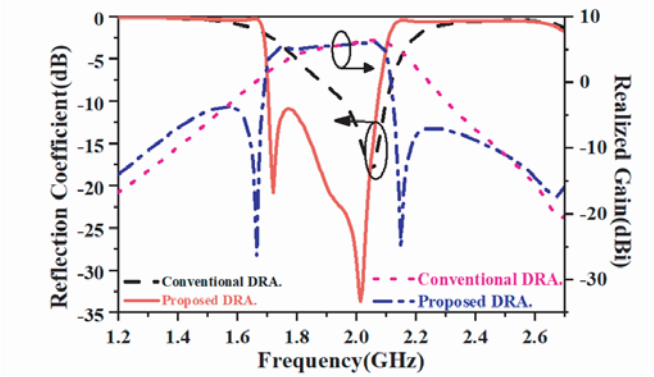

Figure 2. The simulated reflection coefficients and realized broadside gain of the conventional DRA and the proposed DRA.

proposed filtering DRA. The bandwidth is greatly widened (from 7.4% to 19%) by increasing from one resonant point to two when the hybrid feeding structure is introduced. Meanwhile, two radiation nulls are introduced at 1.67 and 2.15 GHz, generating bandpass filtering responses. It can also be seen that the realized broadside gain curve in the passband becomes an almost flat line (around 5.6 dBi), which is related to the broadened impedance bandwidth. The change rates of gain at higher and lower band-edge are 31.5 dB/80 MHz and 30 dB/65 MHz respectively. The shape factor representing the steepness of the change in the frequency response is introduced to evaluate the filtering performance of antenna, which is greater than or equal to one and the less the better [18]. The shape factor ($K = \Delta f_{-25\,\mathrm{dB}}/\Delta f_{-3\,\mathrm{dB}}$) of the proposed antenna is 1.17. The broadside gain of the proposed antenna shows high band-edge selectivity.

2.3. Analysis of the Radiation Nulls

By introducing cross coupling between non-adjacent resonant units, zero poles at specified frequencies in filters are realized. This method can also be applied to design filtering antennas. The transfer function of a cascaded trisection filter could be expressed as

$$|S_{21}| = \frac{1}{\sqrt{1+\chi^2 F_n^2(\Omega)}} \tag{1}$$

$$F_n(\Omega) = \cosh\left[\sum_{i=1}^{n} \cosh^{-1}\left(\frac{\Omega - 1/\Omega_{ai}}{1-\Omega/\Omega_{ai}}\right)\right] \tag{2}$$

where χ is the ripple constant, Ω the frequency variable of the lowpass prototype filter, Ω_{ai} the ith attenuation pole, and n the degree of the filter [19].

The conventional cascaded trisection can generate only one radiation null at the lower or the higher side of passband forming asymmetric filtering characteristics [20]. By introducing two different

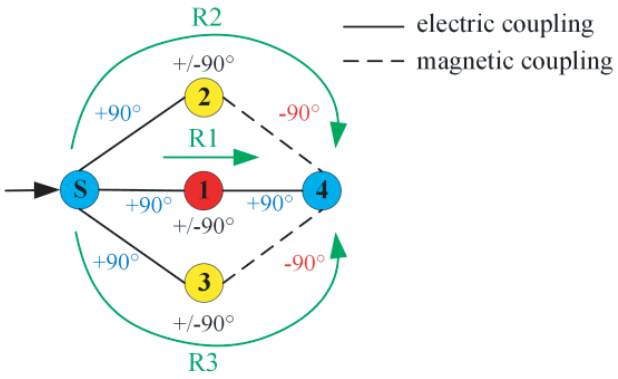

Figure 3. The equivalent coupling topology of the hybrid feeding structure.

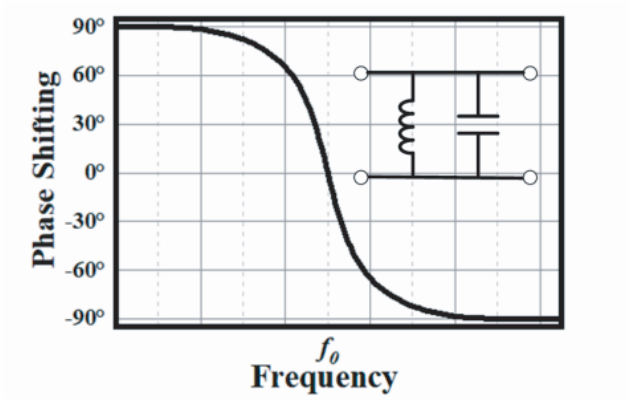

Figure 4. The phase-shifting of a signal while it goes through the resonator.

cascaded trisections to generate two radiation nulls, symmetrical filtering characteristics are obtained in this design. As shown in Figure 3, Ⓢ represents the source sign, ① represents the thin metallic strip on the side of the DR, ② represents the shorter open stub on the bottom of the substrate, ③ represents the longer open stub and ④ represents the DR. Besides, the shorted stub is used for reducing the coupling between the two open stubs to improve the band-edge selectivity.

The microstrip line establishes the electric coupling while the microstrip-coupled slot establishes the magnetic coupling. The source signal is coupled to ①, ②, and ③ through the electric coupling. Then, R1 is coupled from ① to ④ through the electric coupling, while R2 and R3 are coupled from ② or ③ to ④ respectively through the magnetic coupling. Among them, R1 carries half of the total energy, while R2 and R3 carries a quarter of the total energy respectively. It is safe to say that the electrical coupling brings a phase shift of $+90°$, while the magnetic coupling brings the phase shift of $-90°$ [20]. Figure 4 shows a phase shift generated by a parallel resonator. At frequencies lower than the resonant frequency f_0, the phase shift generated by the signal passing through the resonator is $+90°$. At frequencies higher than the resonant frequency f_0, the phase shift is $-90°$.

When signals of different frequencies are input, the phase shifts generated by different coupling paths in Figure 3 are shown in Table 2. At frequencies around 1.67 GHz, the phase shifts generated by R2 and R3 are both 90°. The coupling field from R2 and R3 carries half of the total energy. In addition, the coupling field from R1 carries half of the total energy and 270° phase shift. The coupling fields are of equal amplitude and out-of-phase. Therefore, a radiation null is generated at 1.67 GHz. At frequencies around 1.85 GHz, R2 and R3 generate 90° and −90° phase shifts, respectively. The signal coupled by R2 and R3 is of equal amplitude and out-of-phase. In this situation, no matter how many phase shifts are generated by R1, no radiation null can be generated. At 2.15 GHz, it is similar to 1.67 GHz. R1 generates a 90° phase shift, R2 and R3 both generate a −90° phase shift. Thus, another radiation null is generated at 2.15 GHz.

Table 2. Phase shifts of different frequency.

Frequency	Phase Shifts of R1	Phase Shifts of R2	Phase Shifts of R3
1.67 GHz	$+90° + 90° + 90° = 270°$	$+90° + 90° - 90° = 90°$	$+90° + 90° - 90° = 90°$
1.85 GHz	$+90°$ $(+/-90°)$ $+90° = 270°/90°$	$+90° + 90° - 90° = 90°$	$+90° - 90° - 90° = -90°$
2.15 GHz	$+90° - 90° + 90° = 90°$	$+90° - 90° - 90° = -90°$	$+90° - 90° - 90° = -90°$

For verification of the analysis above, the radiation nulls of the following cases are analyzed as shown in Figure 5: (a) Ant.1: the longer open stub only, (b) Ant.2: the shorter open stub only, (c) Ant.3: the longer and shorter open stubs, (d) the proposed DRA with two open stubs and a shorted stub. Considering the matching issues, the directivity is discussed instead of the realized gain as shown

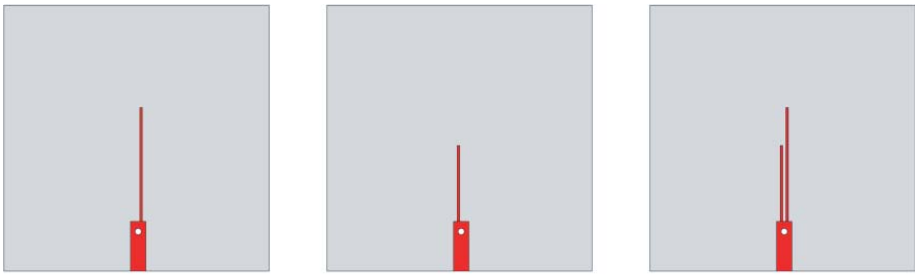

Figure 5. The structure of the bottom of the reference antennas. (a) Ant.1, (b) Ant.2 and (c) reference Ant.3.

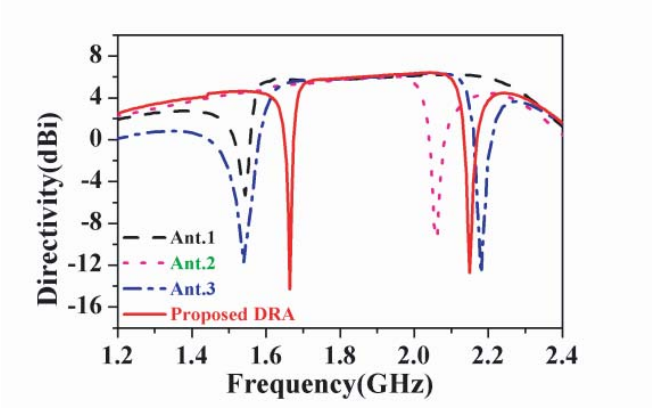

Figure 6. The simulated directivity of the reference antennas and the proposed filtering DRA.

in Figure 6. Ant.1 does not have R2 path in Figure 3, where R1 and R3 share the energy equally. According to Table 2, R1 and R3 generate equal amplitude and out-of-phase electric fields of 270° and 90° respectively at the radiation null around lower band-edge. Similarly, Ant.2 has no R3 path, where R1 and R2 share the energy equally. R1 and R2 generate equal amplitude and out-of-phase electric fields of 90° and −90° respectively at radiation null around higher band-edge. Ant.3 combines Ant.1 and Ant.2 to form two different cascaded trisections, which can generate two radiation nulls at the edge of the passband. However, the radiation null at the higher band edge is shifted from 2.06 GHz to 2.17 GHz, which is due to the influence of the longer open stub on the shorter open stub. By adding a shorted stub to form the proposed DRA, the shorted stub isolates the current between the two open stubs, which weakens the coupling of them in Figure 7. The radiation null at the lower band edge shifts upward while that at the higher band edge shifts downward. This method makes the gain of filtering DRA at the band edge have a big roll-off rate. Therefore, the proposed filtering DRA shows a characteristic of high band-edge selectivity.

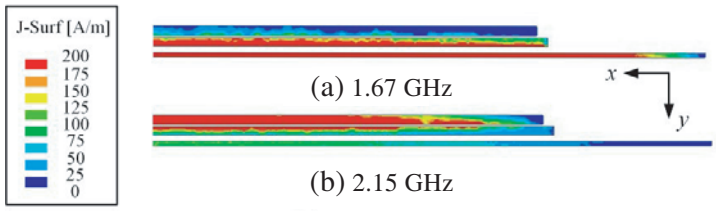

Figure 7. The simulated surface current distribution on the stubs. (a) 1.67 GHz and (b) 2.15 GHz.

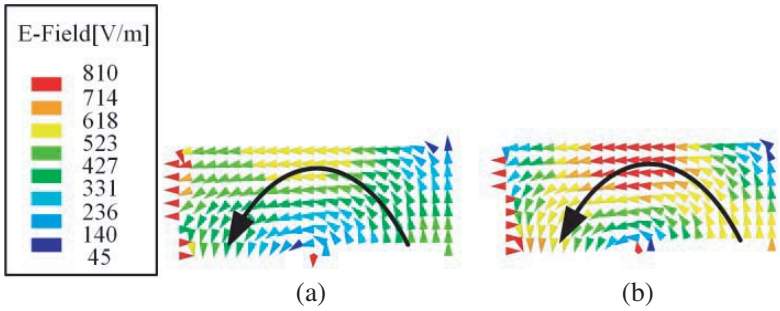

Figure 8. The simulated vector E-filed distribution inside the proposed DRA. (a) 1.72 GHz and (b) 2.07 GHz.

Figure 8 shows the internal electric field of the proposed DRA at different resonant points. It can be seen that the proposed DRA works in the fundamental $TE^{y}_{1\delta1}$ mode of the rectangular DR at the two different resonant frequencies of 1.72 GHz and 2.07 GHz. Two fundamental modes of different frequencies appear due to the perturbation effect of the stubs.

2.4. Parameters Studies

According to the above analysis, the two open stubs with different lengths can adjust the frequencies of the radiation nulls. For verification, the realized broadside gain for different lengths (l_{s1}) of the longer open stub is shown in Figure 9(a). The radiation null at lower band-edge shifts downward with the increasing l_{s1}. Similarly, the radiation null at higher band-edge shifts downward with the increasing l_{s2} of the shorter open stub as shown in Figure 9(b). This is in line with the proposal in the previous section: The radiation null at the lower and the higher band edges can be controlled by the longer and the shorter opened stub respectively. Regarding the impedance matching situation, $l_{s1} = 29.6$ mm and $l_{s2} = 22.1$ mm are finally selected, thus generating two radiation zeros at 1.67 GHz and 2.15 GHz.

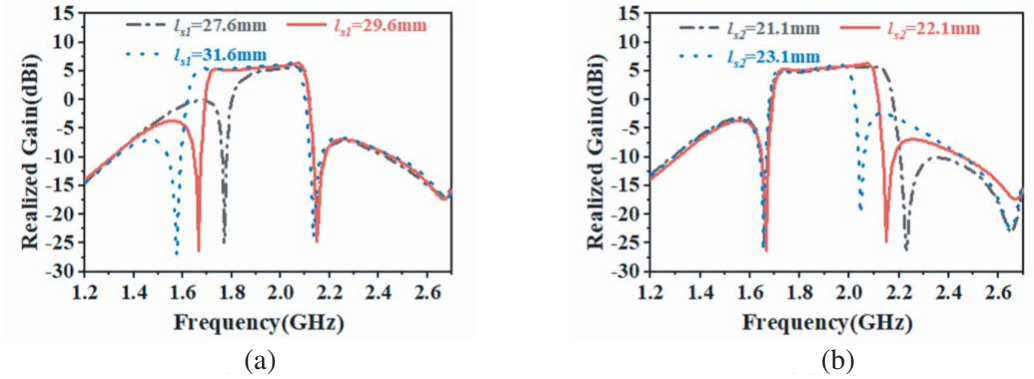

Figure 9. The effects of different stub length on the simulated realized gains. (a) The longer open stub and (b) the shorter open stub.

3. MEASUREMENT RESULTS AND DISCUSSION

For substantiation, a prototype of the proposed filtering DRA is fabricated, as shown in Figure 10. The parameters of the DRA are the same as those in Figure 1. The dielectric resonator consists of a piece of dielectric using alumina ceramic and a thin plate with the same relative permittivity and loss tangent. The thin strip is etched on the thin plate. The size of the dielectric is 45 mm × 44 mm × 17.5 mm,

while that of the thin plate is 45 mm × 1 mm × 17.5 mm. The dielectric resonator was mounted on a Rogers R4003C substrate by glue. The glue layer is also considered in the simulation.

Figure 11 shows the simulated and measured reflection coefficients and broadside gains of the prototype. The measured reflection coefficients and broadside gain slightly deviate towards a higher band with the same trend. The measured broadside gain in the passband has a bigger ripple compared to the simulation. These differences are due to fabrication errors and the discrepancy of the relative permittivity of the dielectric material. The simulated and measured results show that the filtering DRA has a wide bandwidth of 19% and a gain with high band-edge selectivity.

Figure 12 shows the simulated and measured radiation patterns of the prototype at the two resonant

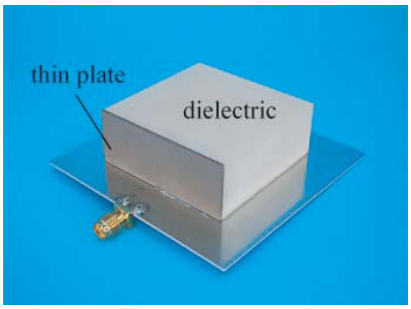

Figure 10. The prototype of the proposed filtering DRA.

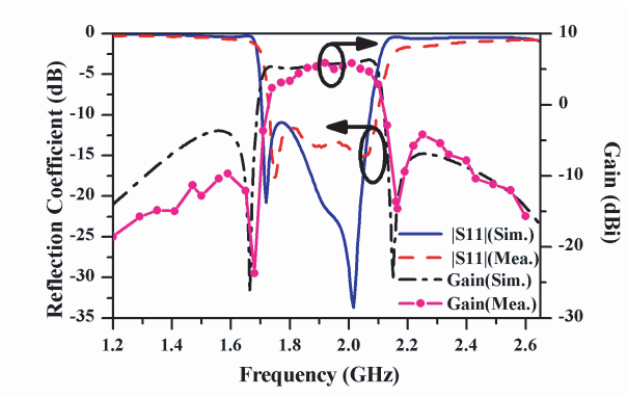

Figure 11. Simulated and measured reflection coefficients and broadside gains of the proposed filtering DRA.

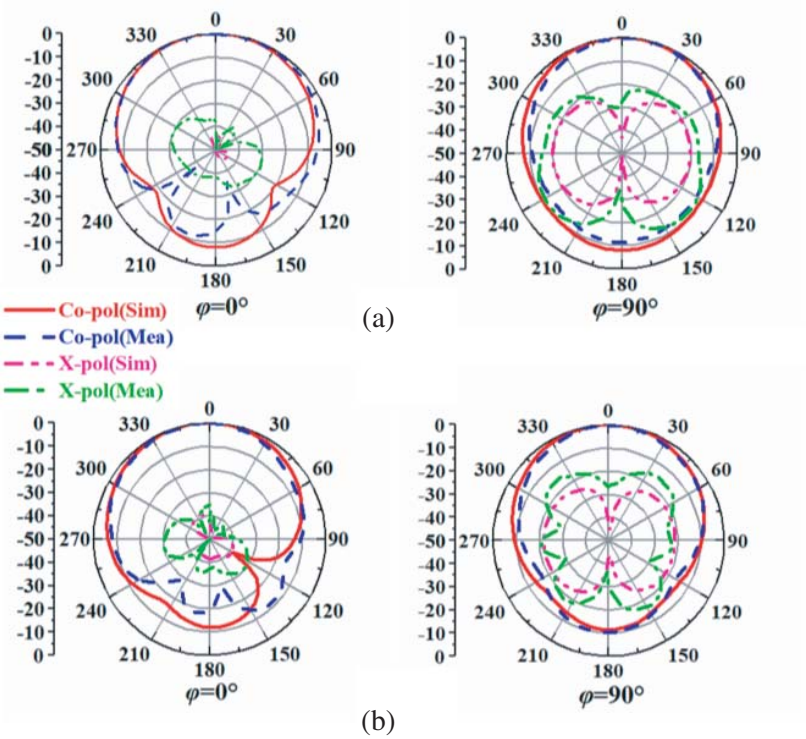

Figure 12. Simulated and measured normalized radiation patterns of the proposed filtering DRA. (a) 1.72 GHz and (b) 2.02 GHz.

frequencies (1.72 GHz and 2.02 GHz). The patterns are stable in the whole passband, where the co-polarized level is stronger than the cross-polarized one by more than -35 dB at $\theta = 0°$.

4. CONCLUSION

In this paper, a filtering rectangle dielectric resonator antenna with high band-edge selectivity is proposed. The proposed DRA is fed by a hybrid feeding structure, which excites two $TE^{y}_{1\delta1}$ modes in different frequencies and realizes a wide bandwidth of 19% (1.71 GHz–2.07 GHz). Besides, the hybrid feeding structure also establishes two different cascaded trisections which introduces two radiation nulls beside the passband and also brings the filtering performance. By introducing a shorted stub, the band-edge selectivity is enhanced. For substantiation, a prototype was fabricated and measured. The results show that the gain and radiation pattern of the filtering DRA remain stable within the passband. A reasonable agreement between the simulated and measured results shows the potential of proposed antenna in wireless communication systems.

ACKNOWLEDGMENT

This work is supported in part by the Fundamental Research Funds for the Central Universities under Grant JB190205.

REFERENCES

1. Xie, B. and H. Yu, "Miniaturized microstrip lowpass filter with ultra-wide stopband performance using trapezoid patch resonators," *Progress In Electromagnetics Research Letters*, Vol. 87, 39–43, 2019.
2. Deng, H. W., T. Xu, and F. Liu, "Broadband pattern-reconfigurable filtering microstrip antenna with quasi-Yagi structure," *IEEE Antennas and Wireless Propagation Letters*, Vol. 17, No. 7, 1127–1131, 2018.
3. Hua, C., X. Jin, and M. Liu, "Design of compact vertically stacked SIW end-fire filtering antennas with transmission zeros," *Progress In Electromagnetics Research Letters*, Vol. 87, 67–73, 2019.
4. Deng, J. Y., S. Hou, L. Zhao, and L. X. Guo, "Wideband-to-narrowband tunable monopole antenna with integrated bandpass filters for UWB/WLAN applications," *IEEE Antennas and Wireless Propagation Letters*, Vol. 16, 2734–3737, 2017.
5. Min, X.-L. and H. Zhang, "Compact filtering antenna based on dumbbell-shaped resonator," *Progress In Electromagnetics Research Letters*, Vol. 69, 51–57, 2017.
6. Hsieh, C.-Y., C.-H. Wu, and T.-G. Ma, "A compact dual-band filtering patch antenna using step impedance resonators," *IEEE Antennas and Wireless Propagation Letters*, Vol. 14, 1056–1059, 2015.
7. Deng, J. and L. Feng, "Dual-band microstrip filtering antennas with symmetrical slots," *Progress In Electromagnetics Research Letters*, Vol. 86, 13–19, 2019.
8. Pan, Y. M., P. Hu, X. Y. Zhang, and S. Y. Zheng, "A low-profile high-gain and wideband filtering antenna with metasurface," *IEEE Transactions on Antennas & Propagation*, Vol. 64, No. 5, 2010–2016, 2016.
9. Bakshi, G., A. Vaish, and R. S. Yaduvanshi, "Two-layer sapphire rectangular dielectric resonator antenna for rugged communications," *Progress In Electromagnetics Research Letters*, Vol. 85, 73–80, 2019.
10. Lu, L., Y.-C. Jiao, H. Zhang, and R. Wang, "Wideband circularly polarized antenna with stair-shaped dielectric resonator and open-ended slot ground," *IEEE Antennas and Wireless Propagation Letters*, Vol. 15, 1755–1758, 2016.
11. Al-Azza, A. A., N. Malalla, F. J. Harackiewicz, and K. Han., "Stacked conical-cylindrical hybrid dielectric resonator antenna for improved ultrawide bandwidth," *Progress In Electromagnetics Research Letters*, Vol. 79, 79–86, 2018.

12. Hu, P., Y. M. Pan, X. Y. Zhang, and S. Y. Zheng, "Broadband filtering dielectric resonator antenna with wide stopband," *IEEE Transactions on Antennas & Propagation*, Vol. 5, No. 4, 2079–2084, 2017.
13. Tang, H., C. Tong, and J.-X. Chen, "Differential dual-polarized filtering dielectric resonator antenna," *IEEE Transactions on Antennas & Propagation*, Vol. 66, No. 8, 4298–4302, 2018.
14. Hu, P., Y. M. Pan, and K. W. Leung, "Wide-/dual-band omnidirectional filtering dielectric resonator antennas," *IEEE Transactions on Antennas & Propagation*, Vol. 66, No. 5, 2622–2627, 2018.
15. Pan, Y. M., P. Hu, and X. Y. Zhang, "Compact single-/dual-polarized filtering dielectric resonator antennas," *IEEE Transactions on Antennas & Propagation*, Vol. 66, No. 9, 4474–4484, 2018.
16. Hu, P., Y. M. Pan, X. Y. Zhang, and B. Hu, "A compact quasi-isotropic dielectric resonator antenna with filtering response," *IEEE Transactions on Antennas & Propagation*, Vol. 67, No. 5, 2622–2627, 2018.
17. Petosa, A., *Dielectric Resonator Antenna Handbook*, Artech House, London, 2007.
18. Ludwig, R., *RF Circuit Design-Theory and Applications*, Prentice Hall, Upper Saddle River, 2000.
19. Hong, J. and M. J. Lancaster, *Microstrip Filters for RF/Microwave Applications*, John Wiley & Sons, Inc., 2001.
20. Thomas, J. B., "Cross-coupling in coaxial cavity filters-a tutorial overview," *IEEE Transactions on Microwave Theory and Techniques*, Vol. 51, No. 4, 1368–1376, 2003.